Physica B 406 (2011) 3551–3555

Contents lists available at ScienceDirect

Physica B

journal homepage: www.elsevier.com/locate/physb

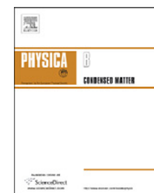

Multiphonon hopping of carriers in CuO thin films

T. Serin [a], A. Yildiz [b,*], Ş.H. Şahin [a], N. Serin [a]

[a] Department of Engineering Physics, Faculty of Engineering, Ankara University, 06100 Ankara, Turkey
[b] Department of Physics, Faculty of Science and Arts, Ahi Evran University, 40040 Kirsehir, Turkey

ARTICLE INFO

Article history:
Received 25 April 2011
Accepted 8 June 2011
Available online 23 June 2011

Keywords:
Sol–gel dip coating technique
CuO
NNH
VRH
MPH

ABSTRACT

We have performed a detailed study of the electrical conduction process in CuO thin films deposited by the sol–gel dip coating technique in a temperature range 280–420 K. The electrical conduction is analyzed within the framework of various hopping conduction models. Multiphonon hopping conduction mechanism is found to dominate the electrical transport in the entire temperature region. Our results are consistent with this model of hopping conduction mechanisms with weak carrier–lattice coupling.

© 2011 Elsevier B.V. All rights reserved.

1. Introduction

The temperature dependence of electrical conductivity forms a key characteristic in the study of charge transport in semiconductor oxide systems. Apart from the optical and structural properties, it is of crucial importance to understand, and hence to tailor, the charge transport processes in these materials. More recently we have studied the electrical conduction properties of various semiconductor oxide systems including TiO_2, SnO_2, Cu_2O and CuO by employing electrical conductivity measurements [1–5]. CuO is a monoclinic structured p-type semiconductor having a band gap of 1.21 eV with promising potential for applications in gas sensors and field effect transistors [6,7]. Although there are a number of experimental and theoretical investigations on the CuO thin films, previous studies have mainly focused on the deposition conditions for the films and their influences on the electrical transports; few authors were concerned about conduction mechanisms in CuO thin films [8,9].

In some cases, variation in the electrical conductivity of the films with temperature cannot be well explained by the classical conductivity of extrinsic semiconductors. In this case, Arrhenius type plots (ln σ vs. T^{-1}) appear to be curved for the films. Several authors take into account that a hopping mechanism is responsible for such a behavior of the electrical conductivity in the CuO thin films [8,9]. However, a clear understanding of the electrical conduction is still lacking and very little is known about the electrical properties of the CuO films. Therefore, it is important from basic understanding as well as from the viewpoint of the devices to investigate how electrical conduction of the CuO thin films is controlled, and this is the main theme of the present investigation. To the best of our knowledge there has been no detailed study using different hopping conduction models to explain the electrical conduction process in the CuO films. Here the electrical conduction properties of the CuO thin films prepared by sol–gel dip coating technique are comprehensively analyzed.

2. Experimental

The films were deposited by the sol–gel dip coating technique on ultrasonically cleaned glass substrates. The coating solution was prepared by dissolving copper acetate [Cu $(CH_3COO)_2 . xH_2O$] in ethanol. Thereafter, lactic acid and triethylamine ($C_6H_{15}N$) were added to the solution. The solution was mixed with a magnetic stirrer for 2 h and was allowed to age for 24 h at room temperature before the deposition on the glass substrate. Film deposition was carried out with a controlled speed of approximately 0.36 cm/s. After coating, the substrates were baked at 300 °C for 5 min in air. The above coating and baking process were repeated for 10–20 times to prepare samples of different thicknesses. Finally the samples were annealed in air at 500 °C for 1 h.

The microstructure of the deposited films was investigated by means of an Inel-EQUINOX 1000 diffractometer. The radiation source, the wavelength and the scanning range 2θ of the diffractometer were CoKα, 0.179 nm and 10–80°, respectively.

The optical band gaps of the films were calculated by means of UV–Vis–NIR transmittance measurements performed with Shimadzu UV-3600 spectrophotometer in the spectral range 300–1500 nm.

* Corresponding author. Tel.: +90 386 252 80 50; fax: +90 386 252 80 54.
E-mail address: yildizab@gmail.com (A. Yildiz).

0921-4526/$ - see front matter © 2011 Elsevier B.V. All rights reserved.
doi:10.1016/j.physb.2011.06.021

The surface morphology of the films was investigated by atomic force microscopy (AFM, in contact mode, PSIA XE-100E).

The electrical resistance measurements were performed, as a function of temperature, with Keithley 2420 programmable constant current source in a temperature range 280–420 K.

3. Results and discussion

The X-ray diffraction patterns for the CuO film are shown in Fig. 1. The spectra show well-resolved two diffraction peaks. These peaks correspond to the reflection of the $(\bar{1}\,1\,1)/(0\,0\,2)$ and the $(2\,0\,0)/(1\,1\,1)$ planes of standard JCPDS data card of CuO [10]. Since all the peaks are sharp it is evident that the films are of polycrystalline structure. The crystallite size for crystallites with $(2\,0\,0)/(1\,1\,1)$ plane was calculated using Scherrer's formula, neglecting peak broadening due to residual stresses in the films, $D=0.9\lambda/(\beta\cos\theta)$ where D is the size of crystallite, β is the broadening of diffraction line measured at half its maximum intensity in radians and λ is the wavelength of X- rays (0.179 nm). The calculated values of crystallite size are obtained as 37.2 Å (for 10 layers) and 76.7 Å (for 20 layers).

The optical band gaps of the films have been determined on the basis of UV–Vis–NIR transmission measurements. For this, the fundamental absorption coefficient (α) was evaluated using $\alpha=(\ln T^{-1})/t$ where t is the film thickness and T is the transmittance. The absorption coefficient value is of the order of 104 cm^{-1} supporting the direct band gap nature of the material. The nature of the direct allowed transition is determined using the following relation:

$$\alpha h\nu = A(h\nu - E_g)^{1/2} \tag{1}$$

where $h\nu$ is the photon energy, E_g the optical band gap energy and A is a constant. The typical plot of $(\alpha h\nu)^2$ vs. $h\nu$ is shown in Fig. 2. It is linear indicating the presence of direct transition. The linear portion is extrapolated to $\alpha=0$, on energy axis, which gives the band gap energy of 1.75 and 1.80 eV for 10 and 20 layers samples, respectively. It has been reported that the band gap of CuO depended on the preparation conditions of CuO in a wide range (1.75–2.15 eV) [11–14].

Fig. 3 shows 2D and 3D surface AFM analyses of the samples. It was observed that the films are polycrystalline and the average grain size increases from 50 to 80 nm with the increasing film thickness. It is also seen that the result is in good agreement with the published general conclusion in the literature, which

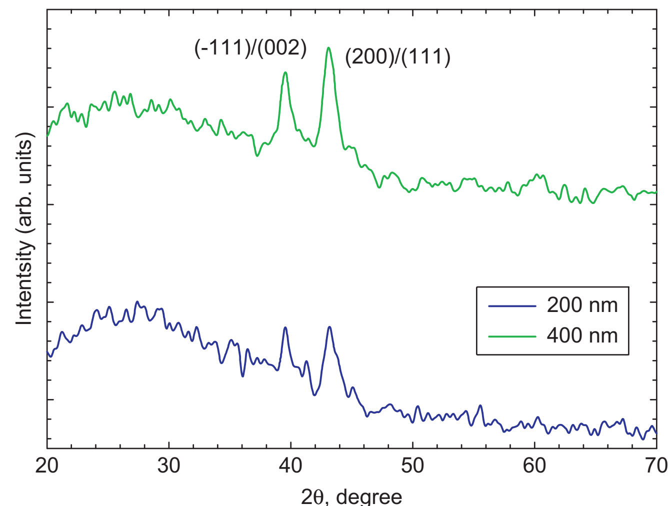

Fig. 1. XRD spectra of the investigated films.

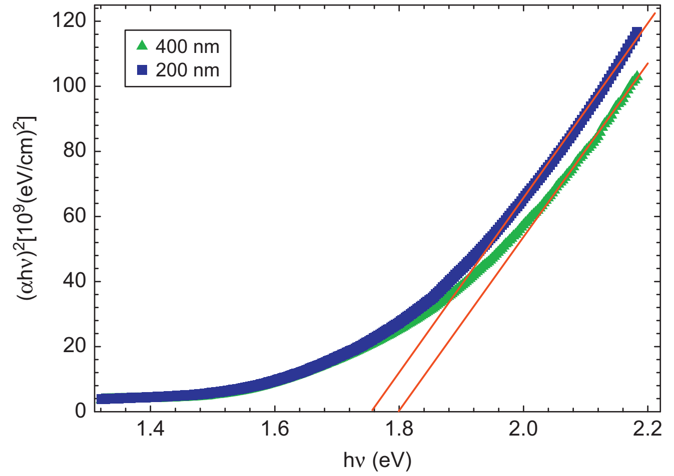

Fig. 2. Plot of $(\alpha h\nu)2$ vs. $h\nu$ for the investigated films.

expresses "the average crystallite size obtained by a large number of experimental data increases with the increasing of the thin film thickness" [15].

Fig. 4 shows the measured electrical conductivity of the CuO thin films with two different thicknesses as a function of temperature. Electrical conductivity of the films strongly depends on the growth conditions. An increase in the conductivity, from the 1.59×10^{-3} to 0.11 $\Omega^{-1}\,cm^{-1}$ at room temperature, is observed with the increase in thickness from 200 to 400 nm. The increase in the conductivity with increasing film thickness may be attributed to deviation from stoichiometry due to the presence of the intrinsic defects such as copper and oxygen vacancies [5].

The generalized conductivity sum [16]

$$\sigma(T) = \sum_i \sigma_{i0}(T)\exp\left[-\left(\frac{T_{i0}}{T}\right)^{s}\right] \tag{2}$$

can be fit to the data of Fig. 4. Here σ_{i0} is the pre-exponential factor and, T_{i0} is a characteristic temperature. The value of $s=1$ corresponds to the conduction in extended states or nearest neighbor hopping (NNH) mechanism. In former case, the conductivity is expressed by the Arrhenius law. In this law, the conductivity is represented by following equation:

$$\sigma(T) = \sigma_{0a}\exp\left(-\frac{E_a}{k_B T}\right) \tag{3}$$

where σ_{0a} is a pre-exponential factor and k_B is Boltzmann's constant. The variation in $\ln\sigma$ with reciprocal temperature highlights an Arrhenius law versus temperature in the investigated temperature range (Fig. 4). The activation energies (E_a) estimated from the slope of the $\ln\sigma=f(10^3/T)$ plot are 0.378 ± 0.003 and 0.193 ± 0.008 eV for thin and thick samples, respectively. One can notice that this parameter decreases with increasing the film thickness.

On the other hand, in the NNH conduction (again $s=1$ in Eq. (2)), carrier hops to the nearest neighbor empty site. For the localized states with an energy separation E_{nn}, which is smaller than the E_a required for thermally activated band to band conduction and the NNH distance r, the hopping probability can be written as [17,18]

$$P_{hop} = \nu_{ph}\exp(-2r/\xi - E_{nn}/k_B T) \tag{4}$$

where ν_{ph} is the phonon frequency associated with hopping process ($\sim10^{13}$ Hz), and ξ is the localization length. The diffusion coefficient D_{hop} for hopping is given by [17,18]

$$D_{hop} = P_{hop} r^2/6 \tag{5}$$

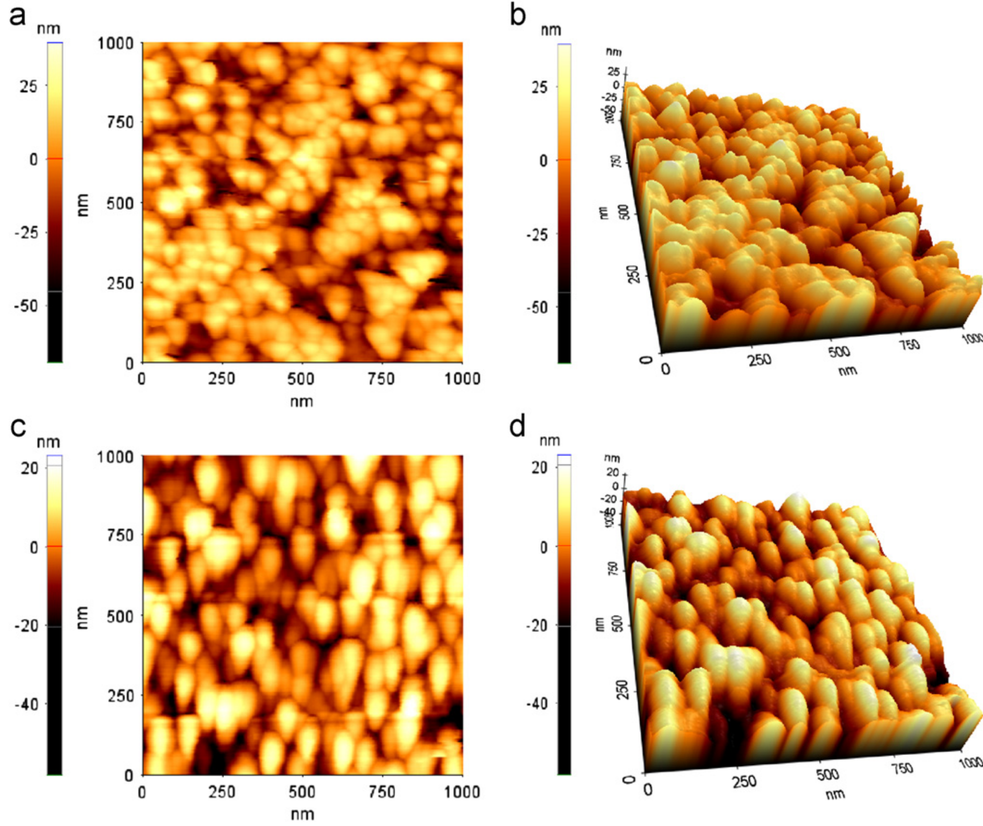

Fig. 3. Two-dimensional (2D) and three-dimensional (3D) AFM images (a) and (b) for thin (200 nm) sample, and (c) and (d) for thick (400 nm) sample.

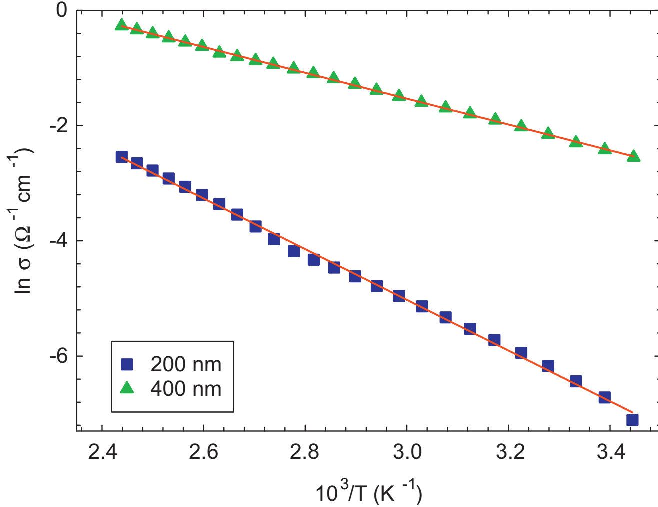

Fig. 4. Arrhenius plot of the films. Solid lines are the best-fit lines with Eq. (3).

Using the Einstein relation, the resistivity can be written as

$$\sigma = e^2 D_{\mathrm{hop}} N(E_{\mathrm{F}}) \tag{6}$$

Combining Eqs. (4)–(6), the temperature dependence of resistivity in the NNH regime is found as [17,18]

$$\sigma = \left[\frac{1}{6} N(E_{\mathrm{F}}) v_{\mathrm{ph}} e^2 r^2\right] \exp(-2r/\xi - E_{\mathrm{nn}}/k_{\mathrm{B}}T) \tag{7}$$

$$\sigma_{\mathrm{nn}}(T) = \sigma_{0\mathrm{n}} \exp\left(-\frac{E_{\mathrm{nn}}}{k_{\mathrm{B}}T}\right) \tag{8}$$

where ($N(E_{\mathrm{F}})$) is the density of states (DOS) and E_{nn} is defined as the average energy needed to hop to the nearest neighbor at a distance r. From simple potential considerations E_{nn} can be estimated using the following equation [19]:

$$E_{\mathrm{nn}} = \frac{e^2 {N_{\mathrm{a}}}^{1/3}}{4\pi\varepsilon} \tag{9}$$

where N_{a} is the acceptor concentration and the static dielectric constant of $\varepsilon = 25$ [20]. Utilizing the values of E_{nn} obtained from Eq. (8), the values of N_{a} are obtained by Eq. (9) as 2.82×10^{23} and 3.76×10^{22} cm^{-3} for thin and thick samples, respectively. These values of N_{a} are unrealistic for the films. Hence, this formalism cannot give a suitable explanation for conduction in the films.

In order to clearly understand the conductivity behavior in the investigated films, results of a numerical evaluation of the differential activation energies are shown in Fig. 5

$$E_{\mathrm{a}} = -k_{\mathrm{B}} \frac{\Delta \ln[\sigma(T)]}{\Delta(1/T)} \tag{10}$$

for successive points in the Arrhenius plot of the data shown in Fig. 4. A fluctuation of the activation energies in the films is observed. On the other hand, the fluctuation of the activation energy is decreased by increasing the film thickness. A single activated term in Eqs. (3) and (8) is therefore inappropriate for the films. This feature may be explained by the single phonon assisted variable-range hopping (VRH) mechanism and is frequently observed in semiconducting oxides [1–5]. With the decreasing temperature, the spatial term in Eq. (4) begins to affect the conductivity. When the phonon energy is insufficient, the more energetic phonon-assisted hops becomes favorable, as a result of which the carriers will tend to hop larger distance in order to locate sites, which are energetically closer than the nearest neighbors. This new regime is known as Mott VRH regime [16].

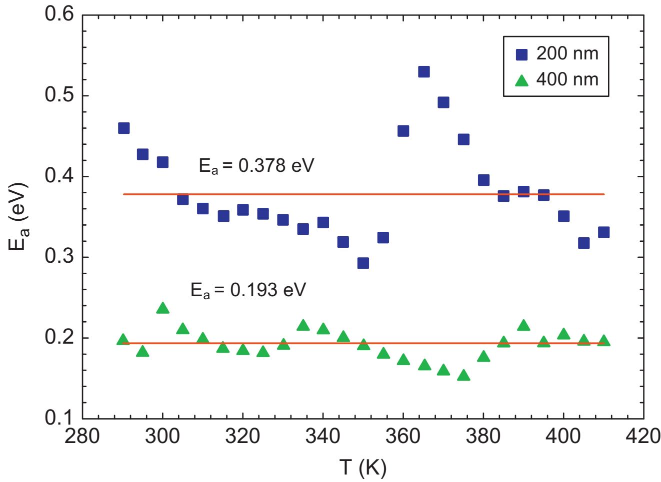

Fig. 5. Double logarithmic plot of the temperature dependence of the differential activation energy E_a (*T*) of the films.

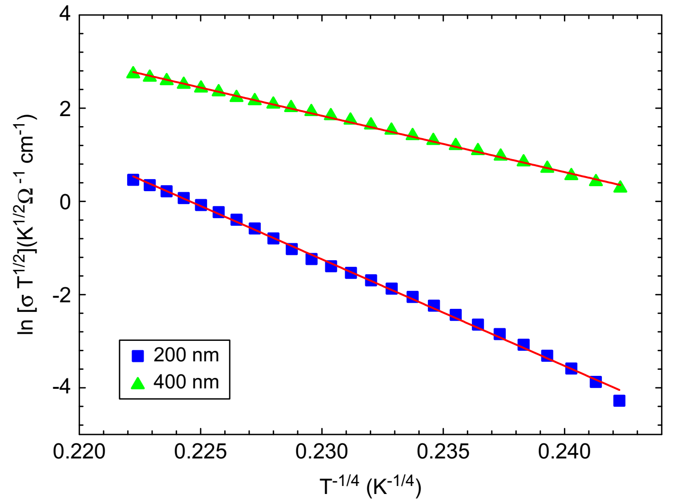

Fig. 6. Temperature dependence of the electrical conductivity plotted as ln ($\sigma T1/2$) vs. $103/T$ for the films. Solid lines are the best-fit lines with Eq. (11).

In this regime, the carrier jumps between more remote defect centers, which are close in energy. In the case of VRH, if the density of states around the Fermi level is assumed to be constant, s becomes s=1/4 in Eq. (2) (Mott VRH) and then conductivity is expressed as [16]

$$\sigma_{vr}(T) = \sigma_{0v} \exp\left[-\left(\frac{T_0}{T}\right)^{1/4}\right] \quad (11)$$

where T_0 is a characteristic temperature coefficient, which depends on the density of states $N(E_F)$ at the Fermi level in the form [16]

$$T_0 = \left[\frac{18}{k_B \xi^3 N(E_F)}\right] \quad (12)$$

where σ_{0v} is given as

$$\sigma_{0v} = \frac{3e^2 \nu_{ph}}{(8\pi)^{1/2}} \left[\frac{\xi N(E_F)}{T}\right]^{1/2} \quad (13)$$

Presentations of the temperature dependence of the conductivity according to Eq. (11) are given in Fig. 6. These graphs show that the VRH conductivity can be found in the entire temperature range of conductivity. The experimental data of the films show a good fit with Mott's formula. The characteristic temperatures T_0 are obtained from linear fits of these plots as $2.74 \times 10^9 \pm 29$ and $2.13 \times 10^8 \pm 15$ K for thin and thick samples, respectively. A good fit of the measured data is essential but not sufficient criterion for applicability of the VRH model. There is an indication of the inappropriate form of these equations results from extraction of the ξ by the simultaneous solution of Eqs. (12) and (13) for the best fits to each of the data sets. The value of pre-exponential factor σ_{0v} is estimated as $2.04 \times 10^{22} \pm 1.71$ and $7.32 \times 10^{12} \pm 1.29\ \Omega^{-1}\ \mathrm{cm}^{-1}$ for thin and thick samples, respectively. These values of σ_{0v} provide unphysical small values for ξ (4.41×10^{-22} and 4.43×10^{-12} nm for thin and thick samples, respectively), compared with the usual semiconducting oxides [1–5,16]. Therefore the VRH model is also unsuitable to explain the conductivity data of these films. Therefore, an alternative approach is necessary to explain the experimental conductivity data for the entire range of temperature of our investigation. Finally, we consider the multiphonon hopping (MPH) conduction model, which suggests that carriers couple with both the optical and acoustical phonons. This model includes both Eqs. (8) and (11) over a certain temperature region [21–23]. The hopping rate due to a multiphonon tunneling of localized carriers with weak coupling is expressed as [21–23]

$$\Gamma = C \exp(-\gamma p) \left[\frac{k_B T}{h\nu_0}\right]^p \quad (14)$$

The conductivity is expressed in the following model:

$$\sigma = \frac{n_c e^2 R^2 \Gamma}{6 k_B T} \quad (15)$$

where $C \sim \nu_0$, $n_c = N(E_F) k_B T$ and $\gamma = \ln(\Delta/E_M)^{-1}$. The parameter E_M or γ is a measure of the carrier–phonon coupling strength. ν_0 is the frequency of the acoustical phonon, which is most effectively coupled to localized electrons. A measure of the number of phonons participating in transport between hopping sites is also given by $p = \Delta/h\nu_0$, with the ratio expressed as the average site energy difference Δ to the average energy $h\nu_0$ of the phonon modes coupled to the electrons. We have from Eqs. (14) and (15)

$$\sigma \alpha (T/T_0)^p \quad (16)$$

The MPH process involves absorption and emission of *p* phonons. Therefore, it should be an integral number but becomes a non-integral number, provided the distribution of hopping site distance is considered. We illustrate the conductivity data of the films in Fig. 7 when the MPH model is considered. The fit with the MPH model is better than both the NNH and Arrhenius, and the VRH fits. However, in light of this model we should check whether the estimated parameters are physically plausible values. The values of $p = 15.4 \pm 0.2$ and 7.8 ± 0.2 and of $\gamma = 5.07 \pm 0.38$ and 7.58 ± 0.32 are calculated from the least squares straight line fits for the thin and thick films, recpectively. These results suggest that the number of phonons involved in the hopping process decreases with increasing film thickness. The single phonon assisted VRH mechanism requires the condition $h\nu_0 > \Delta$. Since the $p > 1$, the condition $h\nu_0 > \Delta$ is not fulfilled for both films namely the VRH cannot take place in the investigated temperature range for the films. According to Emin [23], $\Delta \sim 2E_{nn}$. Using the relation of $p = \Delta/h\nu_0$, ν_0 can be determined as $1.19 \times 10^{13}\ \mathrm{s}^{-1}$. According to the MPH model, the value of ν_0 must be lower than the Debye frequency (ν_D). This condition is satisfied here. We can estimate here the value of ν_D of the studied samples as $1.21 \times 10^{13}\ \mathrm{s}^{-1}$, according to $\theta_D\ k_B = \nu_D$ (θ_D is Debye temperature $\sim$580 K for CuO) [24]. The average lattice separation value of a_0 is approxiamtely given by $(\nu_0/\nu_D)\ a_B^*$, it can be estimated as about 0.165 nm for the films. Here a_B^* is Bohr radius which calculated as $a_B^* = 4\pi\varepsilon h^2/m^* e^2 = 0.167$ nm, where effective mass of $m^* = 7.9 m_0$

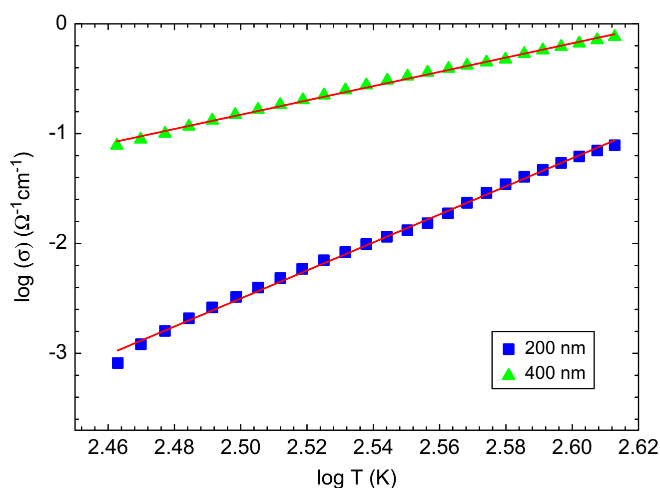

Fig. 7. Temperature dependence of the electrical conductivity plotted as log (σ) vs. log T for the films. Solid lines are the best-fit lines with Eq. (16).

for CuO [25]. This value of a_0 is consistent with the prediction by Robertson [22].

The MPH conduction regime with weak carrier–lattice interaction should satisfy the condition [26]

$$G = (E_M/h\nu_0)(k_BT/h\nu_0) < 1 \quad (17)$$

Using $\gamma = \ln(\Delta/E_M) - 1$, the values of E_M can be obtained as 1.75×10^{-3} and 7.25×10^{-5} eV for the thin and thick films, respectively. This yields $G = 1.86 \times 10^{-2}$ and 7.68×10^{-4} at room temperature for the thin and thick films, respectively. Since the condition (Eq. (17)) is fulfilled here, we conclude that the MPH conduction with weak carrier–lattice interaction is the most probable conduction mechanism in the investigated CuO films.

4. Conclusions

We have studied the electrical conduction properties of CuO films from 420 down to 280 K. The temperature behaviors of conductivity in the films have been carefully analyzed and the conduction mechanisms have been satisfactorily explained. We found that neither the conduction in extended states nor the NNH and the VRH conductions processes in the films can give the correct picture to explain electrical conduction. The electrical conduction in this case was found to be governed by the well-known MPH mechanism.

Acknowledgments

This work was supported by the Ankara University BAP under Project number 2007-07-45-054. We would also like to thank Prof. Dr. Yusuf Kağan Kadıooğlu for providing XRD measurements.

References

[1] A. Yildiz, F. Iacomi, D. Mardare, J. Appl. Phys. 108 (2010) 083701.
[2] A. Yildiz, N. Serin, M. Kasap, T. Serin, D. Mardare, J. Alloys Compd. 493 (2010) 227.
[3] T. Serin, A. Yildiz, N. Serin, N. Yıldırım, F. Özyurt, M. Kasap, J. Electron. Mater. 39 (2010) 1152.
[4] T. Serin, A. Yildiz, Ş.H. Şahin, N. Serin, Physica B 406 (2011) 575.
[5] A. Yildiz, N. Serin, T. Serin, M. Kasap, Opt. Adv. Mater. 3 (2009) 1034.
[6] C. Wang, X.Q. Fu, X.Y. Xue, Y.G. Wang, T.H. Wang, Nanotechnology. 18 (2007) 145506.
[7] L. Liao, Z. Zhang, B. Yan, Z. Zheng, Q.L. Bao, T. Wu, C.M. Li, Z.X. Shen, J.X. Zhang, H. Gong, J.C. Li, T. Yu, Nanotechnology 20 (2009) 085203.
[8] D. Das, T.K. Kundu, M.K. Dey, S. Chakraborty, D. Chakraborty, Proc. Indian Acad. Sci. (Chem. Sci.) 115 (2003) 341.
[9] Y. Zhang, L. Pan, Y. Gu, F. Zhao, H. Qiu, J. Yin, H. Zhu, J.Q. Xiao, J. Appl. Phys. 105 (2009) 086103.
[10] JCPDS Card No 65-2309 (Monoclinic CuO).
[11] L.L. Kazmerski, Polycrystalline and Amorphous Thin Films and Devices, Academic Press, New York, 1980.
[12] E.M. Alkoy, P.J. Kelly, Vacuum 79 (2000) 221.
[13] S.C. Ray, Sol. Energy Mater. Sol. 68 (2001) 307.
[14] J.F. Pierson, A. Thobor-Keck, A. Billard, Appl. Surf. Sci 210 (2003) 359.
[15] M. Nair, L. Guerrero, O. Arenas, P. Nair, Appl. Surf. Sci 150 (1999) 143.
[16] N.F. Mott, E.A. Davis, Electronic Processes in Non-Crystalline Materials, Clarendon Press, Oxford, 1971.
[17] A. Miller, E. Abrahamas, Phys. Rev. 120 (1960) 745.
[18] R.A. Street, Hydrogenated Amorphous Silicon, Cambridge University Press, Cambridge, 1991.
[19] B.I. Shklovskii, Sov. Phys. Semicond. 6 (1973) 1053.
[20] X.G. Zheng, Y. Sakurai, Y. Okayama, T.Q. Yang, L.Y. Zhang, X. Yao, K. Nonaka, C.N. Xu, J. Appl. Phys. 92 (2002) 2703.
[21] D. Emin, Adv. Phys. 24 (1975) 305.
[22] N. Robertson, L. Friedman, Philos. Mag. 33 (1976) 753.
[23] D. Emin, Phys. Rev. Lett. 32 (1974) 303.
[24] A. Junod, D. Eckert, G. Triscone, J. Muller, W. Reichardt, J. Phys.: Condens. Matter 1 (1989) 8021.
[25] T. Ito, H. Yamaguchi, K. Okabe, T. Masumi, J. Mater. Sci. 33 (1998) 3555.
[26] R. Englman, J. Jortner, Mol. Phys. 18 (1970) 145.